2-D Exact Analytical Model for Surface-Mounted Permanent-Magnet Motors With Semi-Closed Slots.

Thierry Lubin, Smail Mezani, Abderrezak Rezzoug

2D Exact Analytical Model for Surface-Mounted Permanent Magnet Motors with Semi-Closed Slots

Thierry Lubin, Smail Mezani, and Abderrezak Rezzoug

Groupe de Recherche en Electrotechnique et Electronique de Nancy,
University Henri Poincaré, Nancy, FRANCE

This paper presents an analytical subdomain model to compute the magnetic field distribution in surface-mounted permanent-magnet (PM) motors with semi-closed slots. The proposed model is sufficiently general to be used with any pole and slot combinations including fractional slot machines with distributed or concentrated windings. The model accurately accounts for armature reaction magnetic field and mutual influence between the slots. The analytical method is based on the resolution of two-dimensional Laplace's and Poisson's equations in polar coordinates (by the separation of variables technique) for each subdomain, i.e. magnet, airgap, slot-opening and slots. Magnetic field distributions, back-EMF and electromagnetic torque (including cogging torque) computed with the proposed analytical method are compared with those issued from finite element analyses.

Index Terms— **Analytical solution, Permanent Magnet Machine, Semi-Closed Slot, Cogging Torque, Armature Reaction Field.**

I. INTRODUCTION

THE stator slotting effect should be considered accurately to predict the magnetic field distribution in the airgap region of PM motors. Indeed, the presence of stator slots has a large influence on the airgap magnetic field and therefore on the motor performances such as radial force and cogging torque which cause noise, speed ripple and vibrations. The airgap magnetic field computation including slotting effects can be evaluated either by numerical approaches like the finite element method or by analytical methods. Analytical methods are, in general, less computational time consuming than numerical ones and can provide closed-form solutions giving physical insight for designers. So, they are useful tools for first evaluation of electrical motors performances and for design optimization.

Different analytical approaches have been developed for the determination of the airgap magnetic field considering slotting effects. Recent comprehensive reviews on this subject can be found in the literature [1], [2] and [3] and will not be developed in detail here. Two analytical methods are mainly used. The first one is based on conformal maping and provides a 2-D relative permeance function to account for slotting effect [4-8]. The second method consists in solving directly the Maxwell's equations in all subdomains (airgap, stator slots and magnets) by the separation of variables technique [1-3] and [9-20]. The magnetic field distribution is obtained in each subdomain by using boundary and interface conditions.

Analytical solutions based on subdomains method which can be found in the literature deal only with open slots PM motors. However, the stator slots are usually semi-closed for low and medium power PM motors. In fact, the modeling of PM motor with open slots is sufficient and gives accurate results when the objective is to study the influence of the slot-opening on the cogging torque [3], [16] under no-load conditions.

Fig. 1. Geometry of a 6-slot /4-pole three-phase PM motor with semi-closed slots and alternate teeth wound ($p = 2$ and $Q = 6$).

However, for the determination of the motor performances under both no-load and load conditions, it is necessary to take into account the more complicated problem of the semi-closed slots geometry as shown in Fig. 1.

In this paper, the authors propose an exact analytical solution of the magnetic field distribution in the airgap of a surface-mounted PM machine. The models given in [2], [3] and [16] have been improved and extended to semi-closed slot machines. The proposed model can be used for PM machines with any pole and slot number combinations including fractional-slot machines with distributed or concentrated windings. Only radially magnetized magnets are considered here. Models with parallel magnetization can be found in [2] and [3]. The developed model takes into account the armature

reaction magnetic field and the mutual influence between the slots. The Laplace and Poisson's equations are solved in each subdomain (airgap, magnets, slot-opening and slot regions) and the solution is obtained using boundary and interface conditions.

The problem description and the assumptions of the model are presented in section II. Section III describes the analytical method for magnetic field calculation in the airgap, permanent magnets and in the slot regions. The back-EMF and torque expressions are developed in section IV. The developed analytical model is then used in section V for magnetic field, back-EMF and electromagnetic torque calculation for both fractional and integer numbers of slots per pole and per phase machines. The analytical results are verified thanks to finite-element computations.

II. MOTOR GEOMETRY AND ASSUMPTIONS

The geometric representation of a three-phase (6-slot/4-pole) PM motor with concentrated windings and semi-closed slots is shown in Fig. 1. The geometrical parameters are the inner radius of the rotor yoke R_1, the radius of the PM surface R_2, the inner and outer radii of the slot-opening R_3 and R_4 respectively, and R_5 is the radius of the slot bottom. The pole-arc to pole-pitch ratio of the PM rotor is α, the number of pole pairs is p. The stator presents Q semi-closed slots with current density J_j in each slot. The slot-opening angle is β and the slot-pitch angle is δ.

The angular position of the ith stator slot-opening is defined as

$$\theta_i = -\frac{\beta}{2} + \frac{2i\pi}{Q} \qquad \text{with} \qquad 1 \le i \le Q \qquad (1)$$

In order to simplify the problem, the following assumptions are made:
- End effects are neglected.
- Stator and rotor iron cores are infinitely permeable.
- Radialy magnetized magnets with a relative recoil permeability $\mu_r = 1$.
- The stator slots have radial sides.

As it can be seen in Fig.1, the whole domain of the field problem is divided into four types of subdomains: the rotor PM subdomain (regions I), the air-gap subdomain (region II), the Q stator slots-opening subdomains (regions i, $i=1,2,....,Q$) and the Q stator slots subdomains (regions j, $j=1,2,....,Q$). The subdomains I and II have annular shapes. The ith slot-opening and the jth slot subdomain shapes are shown respectively in Fig. 2 and Fig. 3.

Due to the presence of electrical current in the slots, a magnetic vector potential formulation is used. The problem is solved in 2D polar coordinates. According to the adopted assumptions, the magnetic vector potential has only one component along the z-direction and only depends on the r and θ coordinates. The notations used in the paper are

$$\boldsymbol{A_I} = A_I(r,\theta) \cdot \boldsymbol{e_z} \qquad \text{for the rotor PM subdomain}$$

$$\boldsymbol{A_{II}} = A_{II}(r,\theta) \cdot \boldsymbol{e_z} \qquad \text{for the airgap subdomain}$$

$$\boldsymbol{A_i} = A_i(r,\theta) \cdot \boldsymbol{e_z} \qquad \text{for the ith slot-opening subdomain}$$

$$\boldsymbol{A_j} = A_j(r,\theta) \cdot \boldsymbol{e_z} \qquad \text{for the jth slot subdomain}$$

III. ANALYTICAL SOLUTION OF MAGNETIC FIELD IN THE DIFFERENT SUBDOMAINS

By using the separation of variables technique, we now consider the solution of Poisson's equations in the PMs and slots subdomains (magnet or current carrying regions) and Laplace's equation in the slot-opening and airgap subdomains (air regions). For the sake of clarity of the general solutions in the different subdomains, we adopt the following notations throughout the paper

$$P_w(u,v) = \left(\frac{u}{v}\right)^w + \left(\frac{v}{u}\right)^w \qquad (2)$$

$$E_w(u,v) = \left(\frac{u}{v}\right)^w - \left(\frac{v}{u}\right)^w \qquad (3)$$

A. Solution of Laplace's Equation in the ith Slot-Opening Subdomain (Region i)

The ith slot-opening subdomain and the associated boundary conditions are shown in Fig. 2. We have to solve the Laplace's equation in a domain of inner radius R_3 and outer radius R_4 delimited by the angles θ_i and $\theta_i + \beta$

$$\frac{\partial^2 A_i}{\partial r^2} + \frac{1}{r}\frac{\partial A_i}{\partial r} + \frac{1}{r^2}\frac{\partial^2 A_i}{\partial \theta^2} = 0 \quad \text{for} \quad \begin{cases} R_3 \le r \le R_4 \\ \theta_i \le \theta \le \theta_i + \beta \end{cases} \qquad (4)$$

The tangential component of the magnetic field at the sides of the slot-opening is null (infinite permeability for the stator iron core). In terms of magnetic vector potential, the boundary conditions for the ith slot domain are

$$\left.\frac{\partial A_i}{\partial \theta}\right|_{\theta=\theta_i} = 0 \qquad \text{and} \qquad \left.\frac{\partial A_i}{\partial \theta}\right|_{\theta=\theta_i+\beta} = 0 \qquad (5)$$
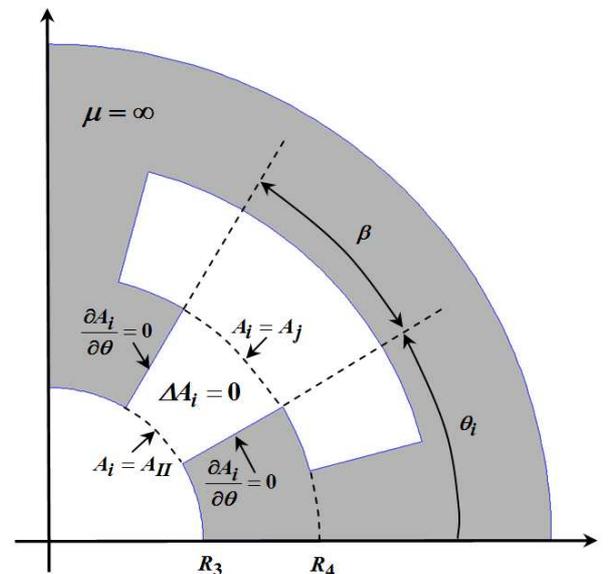

Fig. 2. ith slot-opening subdomain with its boundary conditions.

The continuity of the radial component of the flux density leads to

$$A_i(R_3, \theta) = A_{II}(R_3, \theta) \tag{6}$$

$$A_i(R_4, \theta) = A_j(R_4, \theta) \tag{7}$$

where $A_{II}(r,\theta)$ and $A_j(r,\theta)$ are respectively the magnetic vector potentials in the airgap (24) and in the *j*th slot (17).

Considering the boundary conditions (5) and the continuity conditions (6) and (7), the general solution of (4) can be written as

$$A_i(r, \theta) = A_0^i + B_0^i \ln r$$
$$+ \sum_{k=1}^{\infty} \left(A_k^i \frac{E_{k\pi/\beta}(r, R_4)}{E_{k\pi/\beta}(R_3, R_4)} - B_k^i \frac{E_{k\pi/\beta}(r, R_3)}{E_{k\pi/\beta}(R_3, R_4)} \right) \cdot \cos\left(\frac{k\pi}{\beta} (\theta - \theta_i) \right) \tag{8}$$

where k is a positive integer, $E_{k\pi/\beta}(r, R_4)$ is defined by (3), A_0^i, B_0^i, A_k^i and B_k^i are arbitrary constants.

The constants A_0^i, B_0^i, A_k^i and B_k^i are determined using a Fourier series expansion of the airgap magnetic vector potential $A_{II}(R_3, \theta)$ and the one of the slot magnetic vector potential $A_j(R_4, \theta)$ over the slot-opening interval $[\theta_i, \theta_i + \beta]$.

$$A_0^i + B_0^i \ln R_3 = \frac{1}{\beta} \int_{\theta_i}^{\theta_i + \beta} A_{II}(R_3, \theta) \cdot d\theta \tag{9}$$

$$A_0^i + B_0^i \ln R_4 = \frac{1}{\beta} \int_{\theta_i}^{\theta_i + \beta} A_j(R_4, \theta) \cdot d\theta \tag{10}$$

$$A_k^i = \frac{2}{\beta} \int_{\theta_i}^{\theta_i + \beta} A_{II}(R_3, \theta) \cdot \cos\left(\frac{k\pi}{\beta} (\theta - \theta_i) \right) \cdot d\theta \tag{11}$$

$$B_k^i = \frac{2}{\beta} \int_{\theta_i}^{\theta_i + \beta} A_j(R_4, \theta) \cdot \cos\left(\frac{k\pi}{\beta} (\theta - \theta_i) \right) \cdot d\theta \tag{12}$$

The coefficients A_0^i, B_0^i, A_k^i and B_k^i are developed in the appendix.

B. Solution of Poisson's Equation in the jth Slot Subdomain (Region j)

The *j*th slot domain and its boundary conditions are shown in Fig. 3. We have to solve the Poisson's equation in a domain of inner radius R_4 and outer radius R_5 delimited by the angles $\theta_i + 1/2 \cdot (\beta - \delta)$ and $\theta_i + 1/2 \cdot (\beta + \delta)$

$$\frac{\partial^2 A_j}{\partial r^2} + \frac{1}{r} \frac{\partial A_j}{\partial r} + \frac{1}{r^2} \frac{\partial^2 A_j}{\partial \theta^2} = -\mu_0 J_j \tag{13}$$

where J_j is the current density in the slot *j*.
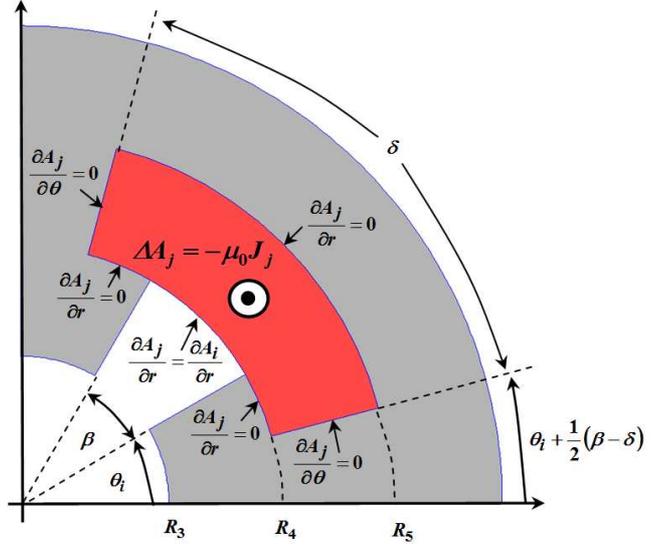
Fig. 3. *j*th slot subdomain with its boundary conditions (with homogeneous current density distribution J_j in the slot)

The tangential component of the magnetic field at the sides and at the bottom of the slot is null (infinite permeability for the stator iron core). The boundary conditions for the *j*th slot domain are then given by

$$\left. \frac{\partial A_j}{\partial \theta} \right|_{\theta = \theta_i + \frac{1}{2}(\beta - \delta)} = 0 \quad \text{and} \quad \left. \frac{\partial A_j}{\partial \theta} \right|_{\theta = \theta_i + \frac{1}{2}(\beta + \delta)} = 0 \tag{14}$$

$$\left. \frac{\partial A_j}{\partial r} \right|_{r = R_5} = 0 \tag{15}$$

As can be seen in Fig. 3, the boundary condition at $r = R_4$ is more complex than the one at $r = R_5$ and must be divided in two parts. A first part corresponds to the stator iron core surface where the tangential component of the magnetic field is null. A second part corresponds to the continuity of the tangential component of the magnetic field between the *j*th slot subdomain and the *i*th slot-opening subdomain. Therefore, the boundary condition at $r = R_4$ can be written as

$$\left. \frac{\partial A_j}{\partial r} \right|_{r = R_4} = \begin{cases} \left. \dfrac{\partial A_i}{\partial r} \right|_{r = R_4} & \forall \theta \in [\theta_i, \theta_i + \beta] \\ 0 & elsewhere \end{cases} \tag{16}$$

According to the superposition principle, the general solution of (13) is the sum of the general solution of the corresponding Laplace's equation and a particular solution [24]. Taking into account the boundary conditions (14), (15) and (16), the solution can be written as

$$A_j(r, \theta) = A_0^j + \frac{1}{2} \mu_0 J_j \left(R_5^2 \ln r - \frac{1}{2} r^2 \right)$$
$$+ \sum_{m=1}^{\infty} A_m^j \cdot \frac{\delta R_4}{m\pi} \cdot \frac{P_{m\pi/\delta}(r, R_5)}{E_{m\pi/\delta}(R_4, R_5)} \cdot \cos\left(\frac{m\pi}{\delta} \left(\theta - \theta_i - \frac{1}{2} (\beta - \delta) \right) \right) \tag{17}$$

where m is a positive integer. The constant A_m^j is determined using a Fourier series expansion of $\left.\dfrac{\partial A_i}{\partial r}\right|_{R4}$ over the slot interval at $r=R_4$

$$A_m^j = \frac{2}{\delta} \int_{\theta_i}^{\theta_i+\beta} \left.\frac{\partial A_i}{\partial r}\right|_{R4} \cdot \cos\left(\frac{m\pi}{\delta}\left(\theta - \theta_i - \frac{1}{2}(\beta - \delta)\right)\right) \cdot d\theta \quad (18)$$

The interface condition (16) also provides a direct relation between the coefficient B_0^i defined in (8) and the current density J_j

$$B_0^i = \frac{\delta}{\beta} \cdot \frac{1}{2} \mu_0 J_j \cdot \left(R_5^2 - R_4^2\right) \quad \text{with} \quad i = j \quad (19)$$

The development of (18) is given in the appendix.

C. Solution of Laplace's Equation in the AirGap Subdomain (Region II)

The airgap subdomain and the associated boundary conditions are shown in Fig. 4. The problem to solve is

$$\frac{\partial^2 A_{II}}{\partial r^2} + \frac{1}{r}\frac{\partial A_{II}}{\partial r} + \frac{1}{r^2}\frac{\partial^2 A_{II}}{\partial \theta^2} = 0 \quad \text{for} \quad \begin{cases} R_2 \leq r \leq R_3 \\ 0 \leq \theta \leq 2\pi \end{cases} \quad (20)$$

The continuity of the tangential component of the magnetic field at $r = R_2$ leads to:

$$\left.\frac{\partial A_{II}}{\partial r}\right|_{r=R_2} = \left.\frac{\partial A_I}{\partial r}\right|_{r=R_2} \quad (21)$$

The boundary condition at the radius $r = R_3$ is more complex because of the existence of the slots as shown in Fig. 1. Considering the continuity of the tangential magnetic field at the interface between the slot-opening and the airgap and considering that the tangential magnetic field is equal to zero elsewhere (infinite permeability of the stator core), the boundary condition at $r = R_3$ can be written as [20]

$$\left.\frac{\partial A_{II}}{\partial r}\right|_{r=R_3} = f(\theta) \quad (22)$$

With

$$f(\theta) = \begin{cases} \left.\dfrac{\partial A_i}{\partial r}\right|_{r=R_3} & \forall \theta \in [\theta_i, \theta_i + \beta] \\ 0 & elsewhere \end{cases} \quad (23)$$

where $A_i(r, \theta)$ is the magnetic vector potential in the *i*th slot-opening given by (8).
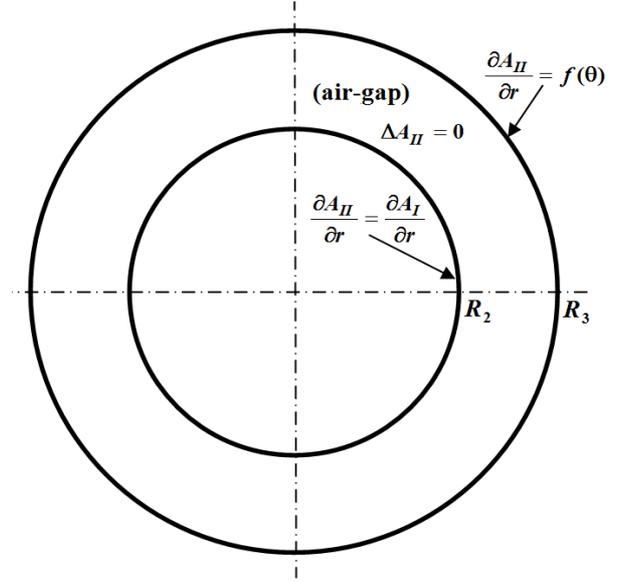
Fig. 4. Airgap subdomain (region II) with its boundary conditions.

Taking into account the boundary conditions (21) and (22), the general solution of the magnetic vector potential in the airgap can be written as

$$A_{II}(r, \theta) = \sum_{n=1}^{\infty} \left(A_n^{II} \frac{R_2}{n} \frac{P_n(r, R_3)}{E_n(R_2, R_3)} + B_n^{II} \frac{R_3}{n} \frac{P_n(r, R_2)}{E_n(R_3, R_2)}\right) \cos(n\theta)$$
$$+ \sum_{n=1}^{\infty} \left(C_n^{II} \frac{R_2}{n} \frac{P_n(r, R_3)}{E_n(R_2, R_3)} + D_n^{II} \frac{R_3}{n} \frac{P_n(r, R_2)}{E_n(R_3, R_2)}\right) \sin(n\theta)$$
$$(24)$$

where *n* is a positive integer, $P_n(r, R_3)$ and $E_n(R_2, R_3)$ are defined by (2) and (3). The coefficients A_n^{II}, B_n^{II}, C_n^{II} and D_n^{II} are determined using Fourier series expansion

$$A_n^{II} = \frac{2}{2\pi} \int_0^{2\pi} \left.\frac{\partial A_I}{\partial r}\right|_{R_2} \cdot \cos(n\theta) \cdot d\theta \quad (25)$$

$$B_n^{II} = \frac{2}{2\pi} \int_0^{2\pi} f(\theta) \cdot \cos(n\theta) \cdot d\theta \quad (26)$$

$$C_n^{II} = \frac{2}{2\pi} \int_0^{2\pi} \left.\frac{\partial A_I}{\partial r}\right|_{R_2} \cdot \sin(n\theta) \cdot d\theta \quad (27)$$

$$D_n^{II} = \frac{2}{2\pi} \int_0^{2\pi} f(\theta) \cdot \sin(n\theta) \cdot d\theta \quad (28)$$

The expressions of the coefficients A_n^{II}, B_n^{II}, C_n^{II} and D_n^{II} are given in the appendix

The radial and tangential flux density distribution in the airgap can be deduced from the magnetic vector potential by

$$B_{IIr} = \frac{1}{r}\frac{\partial A_{II}}{\partial \theta} \qquad B_{II\theta} = -\frac{\partial A_{II}}{\partial r} \quad (29)$$

D. Solution of Poisson's Equation in the PMs Subdomain (Region I)

The rotor PMs subdomain and the associated boundary conditions are shown in Fig. 5. The problem to solve is

$$\frac{\partial^2 A_I}{\partial r^2} + \frac{1}{r}\frac{\partial A_I}{\partial r} + \frac{1}{r^2}\frac{\partial^2 A_I}{\partial \theta^2} = \frac{\mu_0}{r}\frac{\partial M_r}{\partial \theta} \quad \text{for} \quad \begin{cases} R_1 \le r \le R_2 \\ 0 \le \theta \le 2\pi \end{cases} \quad (30)$$

where μ_0 is the permeability of the vacuum and M_r is the radial magnetization of the magnets.

Knowing that the tangential component of the flux density at $r = R_1$ is null (rotor core with infinite permeability) and considering the continuity of the radial component of the flux density at $r = R_2$, we have

$$\left.\frac{\partial A_I}{\partial r}\right|_{r=R_1} = 0 \quad (31)$$

$$A_I(R_2,\theta) = A_{II}(R_2,\theta) \quad (32)$$

The magnetization distribution M_r is plotted in Fig. 6, where B_r is the remanence of the magnets and Δ is the position of the rotor. The radial magnetization can be expressed in Fourier's series and replaced in (30).

Taking into account the boundary conditions (31) and (32), the general solution of the magnetic vector potential in the PMs subdomain can be written as

$$A_I(r,\theta) = \sum_{n=1}^{\infty}\left(A_n^I \frac{P_n(r,R_1)}{P_n(R_2,R_1)} + X_n(r)\cos(n\Delta) \right)\cos(n\theta)$$

$$+ \sum_{n=1}^{\infty}\left(C_n^I \frac{P_n(r,R_1)}{P_n(R_2,R_1)} + X_n(r)\sin(n\Delta) \right)\sin(n\theta) \quad (33)$$

Where

$$X_n(r) = -\frac{P_n(r,R_1)}{P_n(R_2,R_1)}\left(\frac{R_1}{n}\left(\frac{R_1}{R_2}\right)^n f_n'(R_1) + f_n(R_2) \right)$$

$$+ \left(\frac{R_1}{n}\left(\frac{R_1}{r}\right)^n f_n'(R_1) + f_n(r) \right) \quad (34)$$

And

$$f_n(r) = \begin{cases} \dfrac{4B_r p}{\pi(1-n^2)} r \cdot cos\left(\dfrac{n\pi}{2p}(1-\alpha)\right) & if \ n = lp \ \ with \ l = 1, 3... \\[3mm] \dfrac{2B_r}{\pi} r \ln r \cdot cos\left(\dfrac{\pi}{2}(1-\alpha)\right) & if \ n = p = 1 \\[3mm] 0 & otherwise \end{cases}$$

$$(35)$$

where n is a positive integer, p is the number of pole-pairs of the PM rotor and $P_n(r,R_1)$ is defined by (2). It is worth to mention here that the magnetic vector potential solution (33) contains some harmonic terms which are not multiple of the pole pairs number p. This is due to the presence of the slots.

The coefficients A_n^I and C_n^I are determined using a Fourier series expansion of $A_{II}(R_2,\theta)$ over the interval $[0, 2\pi]$

$$A_n^I = \frac{2}{2\pi}\int_0^{2\pi} A_{II}(R_2,\theta)\cdot\cos(n\theta)\cdot d\theta \quad (36)$$

$$C_n^I = \frac{2}{2\pi}\int_0^{2\pi} A_{II}(R_2,\theta)\cdot\sin(n\theta)\cdot d\theta \quad (37)$$

The expressions of the coefficients A_n^I and C_n^I are given in the appendix.
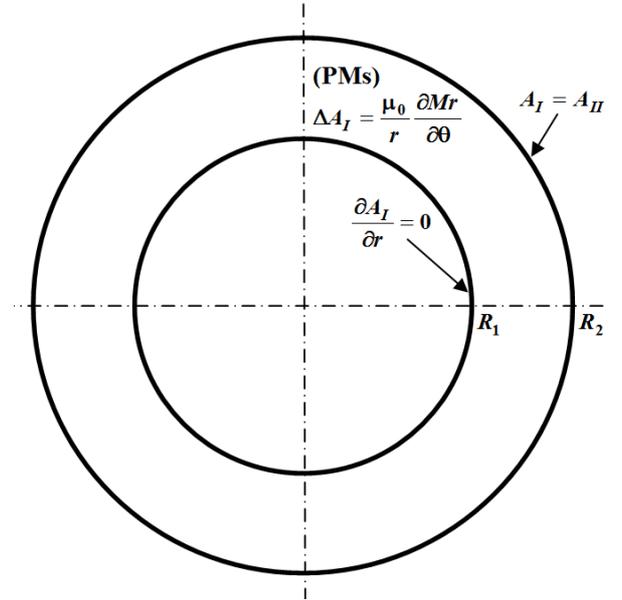
Fig. 5. PMs subdomain (region I) with its boundary conditions.
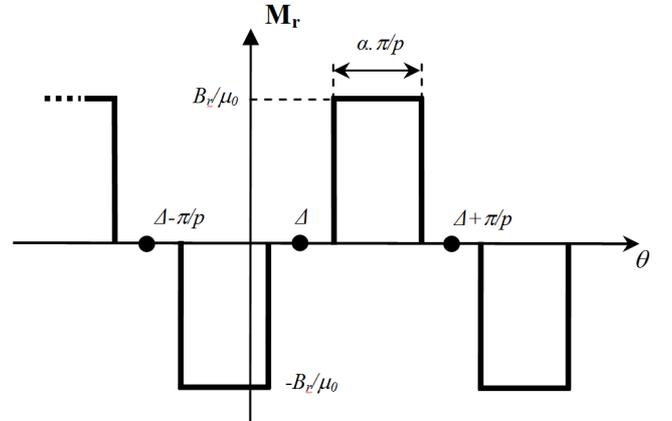
Fig. 6. Magnetization distribution along θ-direction (PM rotor).

IV. BACK-EMF AND TORQUE CALCULATION

A. Electromagnetic torque Calculation

The electromagnetic torque is obtained using the Maxwell stress tensor. A circle of radius R_e in the airgap subdomain is taken as the integration path so the electromagnetic torque is expressed as follows

$$T_e = \frac{LR_e^2}{\mu_0} \int_0^{2\pi} B_{IIr}(R_e, \theta) \cdot B_{II\theta}(R_e, \theta) \cdot d\theta \qquad (38)$$

where L is the axial length of the motor. Substituting (29) into the previous equation, the analytical expression for the electromagnetic torque becomes [20]

$$T_e = \frac{\pi L R_e^2}{\mu_0} \sum_{n=1}^{\infty} (W_n X_n + Y_n Z_n) \qquad (39)$$

Where

$$
\begin{aligned}
W_n &= -A_n^{II} \frac{R_2}{R_e} \frac{P_n(R_e, R_3)}{E_n(R_2, R_3)} - B_n^{II} \frac{R_3}{R_e} \frac{P_n(R_e, R_2)}{E_n(R_3, R_2)} \\
X_n &= -C_n^{II} \frac{R_2}{R_e} \frac{E_n(R_e, R_3)}{E_n(R_2, R_3)} - D_n^{II} \frac{R_3}{R_e} \frac{E_n(R_e, R_2)}{E_n(R_3, R_2)} \\
Y_n &= C_n^{II} \frac{R_2}{R_e} \frac{P_n(R_e, R_3)}{E_n(R_2, R_3)} + D_n^{II} \frac{R_3}{R_e} \frac{P_n(R_e, R_2)}{E_n(R_3, R_2)} \\
Z_n &= -A_n^{II} \frac{R_2}{R_e} \frac{E_n(R_e, R_3)}{E_n(R_2, R_3)} - B_n^{II} \frac{R_3}{R_e} \frac{E_n(R_e, R_2)}{E_n(R_3, R_2)}
\end{aligned}
\qquad (40)
$$

B. Back-EMF Calculation

In order to compute the back-EMF of a 3-phase motor, we first determine at a given rotor position Δ, the flux over each slot j of cross section S_{slot}. We have supposed that the current density is uniformly distributed over the slot area, so the vector potential can be averaged over the slot area to represent the coil

$$\varphi_j = \frac{L}{S_{slot}} \iint_{S_{slot}} A_j(r, \theta) r \, dr \, d\theta \quad \text{with} \quad S_{slot} = \delta \cdot \frac{(R_5^2 - R_4^2)}{2} \quad (41)$$

where L is the machine axial length. The vector potential $A_j(r, \theta)$ is given by (17). The development of (41) gives

$$
\varphi_j = L \cdot A_0^j +
$$
$$
J_j \frac{\delta \mu_0 L}{2 S_{slot}} \left(R_5^4 \left(\ln(R_5) - \frac{5}{8} \right) + R_5^2 R_4^2 \left(\frac{1}{2} - \ln(R_4) \right) + \frac{1}{8} R_4^4 \right) \quad (42)
$$

Under no-load condition ($J_j = 0$), the flux over each slot becomes

$$\varphi_j = L \cdot A_0^j \qquad (43)$$

The phase flux vector is given by

$$
\begin{pmatrix} \Psi_a \\ \Psi_b \\ \Psi_c \end{pmatrix} = n_{turn} \cdot [C] \cdot \begin{pmatrix} \varphi_1 & \varphi_2 & \cdots & \varphi_{Q-1} & \varphi_Q \end{pmatrix} \qquad (44)
$$

where n_{turn} is the number of turns in series per phase and $[C]$ is a connecting matrix (of dimension 3×Q) that represents the stator windings distribution in the slots. The connecting matrix (of the slots with respect to the phases) corresponding to the three-phase PM motor shown in Fig.1 (with 6 stator slots, concentrated windings and alternate teeth wound) is given by

$$
[C] = \begin{bmatrix} 1 & -1 & 0 & 0 & 0 & 0 \\ 0 & 0 & 0 & 0 & 1 & -1 \\ 0 & 0 & 1 & -1 & 0 & 0 \end{bmatrix} \qquad (45)
$$

The three-phase back-EMF vector is computed by

$$
\begin{pmatrix} E_a \\ E_b \\ E_c \end{pmatrix} = \Omega \cdot \frac{d}{d\Delta} \begin{pmatrix} \Psi_a \\ \Psi_b \\ \Psi_c \end{pmatrix} \qquad (46)
$$

where Ω is the rotating speed of the rotor.

V. ANALYTICAL RESULTS AND COMPARISON WITH FINITE ELEMENT CALCULATION

A. Example 1: Fractional slot/pole machine (q=0.5)

As an example of PM machine, we investigate here the performances of a three-phase fractional-slot PM motor shown in Fig.1. This machine presents 4-pole/6-slot corresponding to a number of slot per pole and per phase equal to $q = 0.5$ and a concentrated stator windings with alternate teeth wound. Fractional-slot PM machines with concentrated windings present several advantages such as short end turns and hence a low copper losses, high power density and low cogging torque [21]. Recently, they have found many applications such as domestic and automotive appliances. However, this type of machine presents more important eddy-current losses in the rotor magnets due to the presence of high-level space-harmonics in the armature reaction magnetic field [22]-[23].

The geometrical parameters of the studied PM motor are given in Table I. The analytical solutions in the airgap, in the slots-opening and in the slot domains have been computed with a finite number of harmonic terms N, K and M as indicated in Table I. In order to validate the proposed model, the analytical results have been compared with 2D finite element simulations obtained using FEMM software [25]. The finite-element solutions were obtained by imposing the natural Neumann boundary condition at the surface of the stator and rotor iron cores. The mesh in the different subdomains has been refined until convergent results are obtained.

1) Results for No-Load Condition (B_r = 1.2T and J_{rms}=0 A/mm²)

Figure 7 shows the magnetic flux distribution in the machine under no-load condition. The slot-opening to slot pitch ratio is fixed to $\beta/\delta=0.4$ ($\delta = 30°$ and $\beta = 12°$).

The radial and tangential component of the flux density distribution in the middle of the air-gap (at $r = 2.75cm$) are shown in Fig. 8. The effect of the slots is very clear. One can see the distortion of the flux density waveforms at the location of the slot-opening. An excellent agreement with the results deduced from FEM is obtained. The effect of the slot-opening on the radial component waveform of the flux density is seen in Fig. 9. Indeed, a high value of β (at constant δ) leads to an important variation of the flux density under the slot opening.

The back-EMF waveform as a function of the rotor position for n_{turn}=1 is presented in Fig. 10. The computation is done for a rotating speed $\Omega = 1500$ rpm. The analytical and numerical results are again in close agreement.
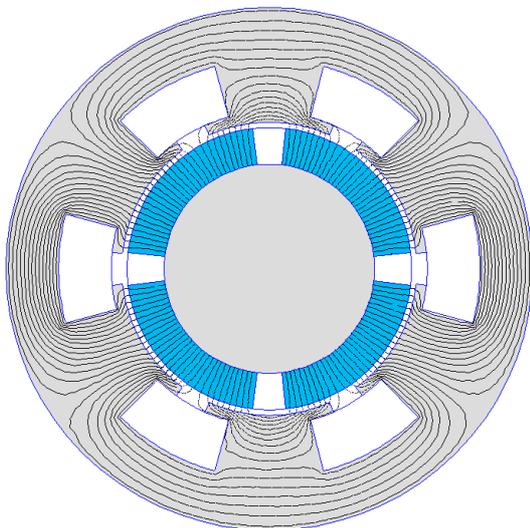
Fig. 7. Magnetic flux distribution for no-load condition ($\beta/\delta = 0.4$).

TABLE I
PARAMETERS OF THE FRACTIONAL SLOT/POLE MACHINE

Symbol	Quantity	value
R_1	Inner radius of the rotor yoke	2 cm
R_2	Radius of the PMs rotor surface	2.7 cm
R_3	Stator bore radius	2.8 cm
R_4	Outer radius of the slot-opening	3 cm
R_5	Outer radius of the slot	4 cm
L	Axial length	10 cm
δ	Slot pitch angle	$\pi/Q = 30°$
β	Slot-opening angle	*variable*
α	PMs pole-arc to pole-pitch ratio	0.85
B_r	Remanence of the permanent magnets	1.2 T
p	Pole-pairs number	2
Q	Number of stator slots	6
J_{rms}	RMS current density	4.6 A/mm²
N	Number of harmonics used for magnetic field calculation in the airgap and PMs domains	100
M	Number of harmonics used for magnetic field calculation in the slot domain	100
K	Number of harmonics used for magnetic field calculation in the slot-opening domain	100

(a)

(b)
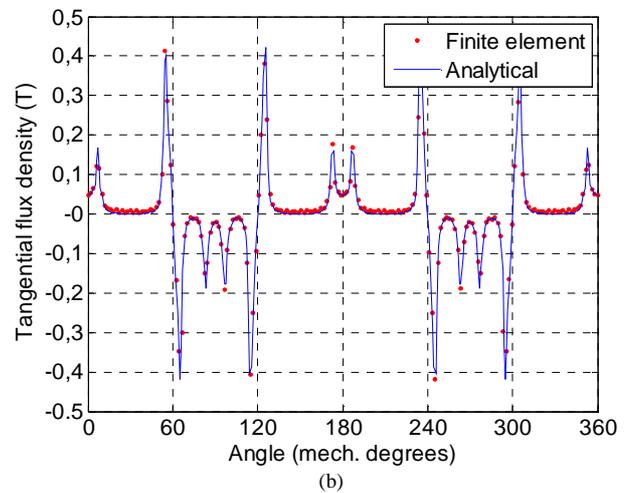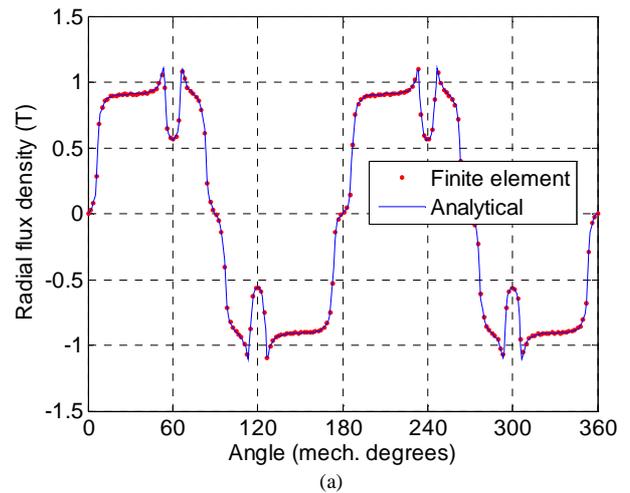
Fig. 8. Radial (a) and tangential (b) component of the flux density at no load in the middle of the airgap for $\beta/\delta = 0.4$
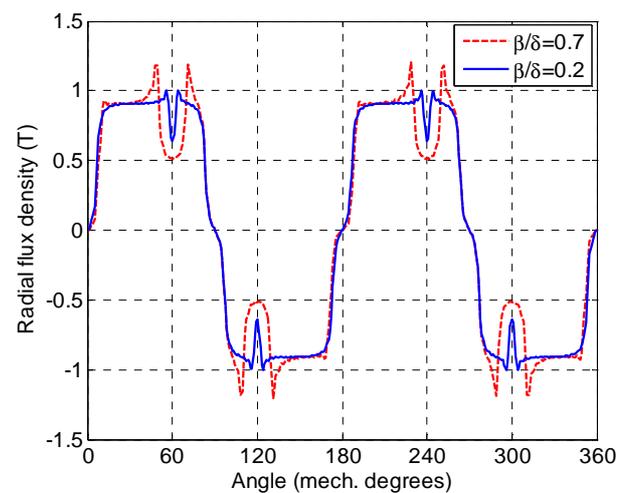
Fig. 9. Radial component of the flux density at no load in the middle of the airgap for $\beta/\delta = 0.2$ and $\beta/\delta = 0.7$, analytical results.

An important characteristic of PM motors is the cogging torque. For a ratio $\beta/\delta = 0.4$, the obtained cogging torque as a function of the mechanical angle is given in Fig. 11. The angular period of the cogging torque corresponds to the Least Common Multiple of $2p$ and Q giving $360°/LCM(4,6)=30°$. The influence of the slot-opening on the cogging torque for several values of β/δ is shown in Fig. 12. As expected, the cogging torque decreases for lower values of the slot-opening. It can be seen that the proposed analytical model can predict the cogging torque with an excellent precision whatever the slot-opening value.

2) Armature Reaction Field ($B_r = 0T$ and $J_{rms}=4.6A/mm²$)
Figure 13 shows the flux distribution in the machine caused by the armature reaction acting alone. The magnets are considered to be unmagnetized and have no effect on the field distribution. The three-phase stator windings are fed with electrical current such as $I_a= I$ and $I_b = I_c =-I/2$ corresponding to AC operation. The radial and tangential components of the armature reaction field in the middle of the air-gap for $\beta/\delta = 0.4$ are plotted in Fig. 14. Very good agreement could be observed between the analytical and the finite-element results.

Using (8) and (17), the radial and tangential components of the flux density distribution in the middle of the slot-opening (at $r = 2.9cm$) and in the middle of the slot domain (at $r = 3.5cm$) are calculated and plotted respectively in Fig. 15 and Fig. 16. It is apparent from these results that the proposed analytical model can predict with an excellent precision the magnetic field distribution in the slot regions and can be used to compute the slot leakage inductance of the machine.

Fig. 10. Per turn phase back-EMF waveform for $\beta/\delta = 0.4$ ($\beta = 12°$)
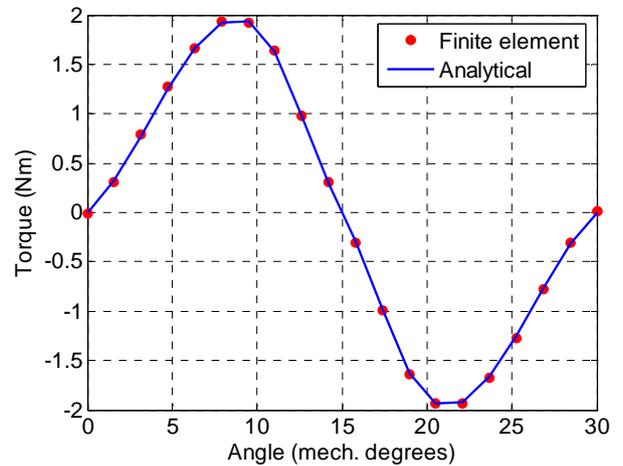
Fig. 11. Cogging torque waveform for $\beta/\delta = 0.4$ ($\beta = 12°$)

Fig. 13. Armature reaction magnetic flux distribution for $J_{rms}=4.6A/mm²$ and $\beta/\delta = 0.4$
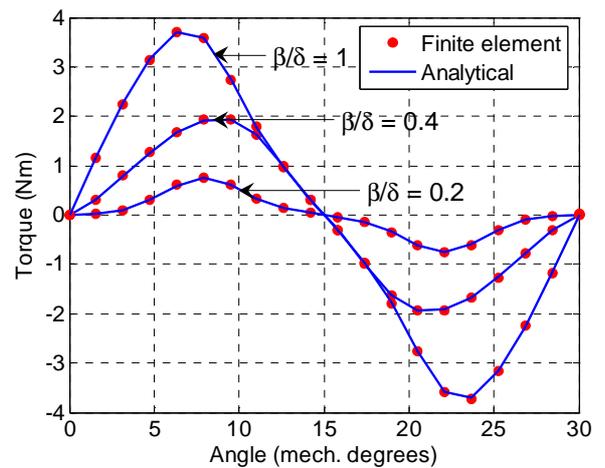
Fig. 12. Cogging torque waveforms for several slot-opening values ($\beta/\delta =1$ corresponds to open slot)
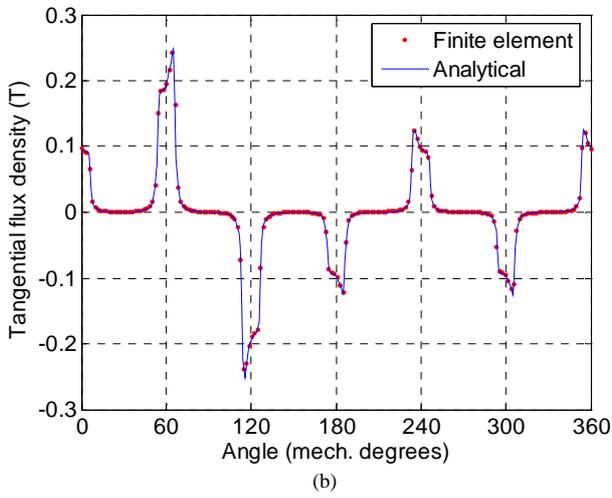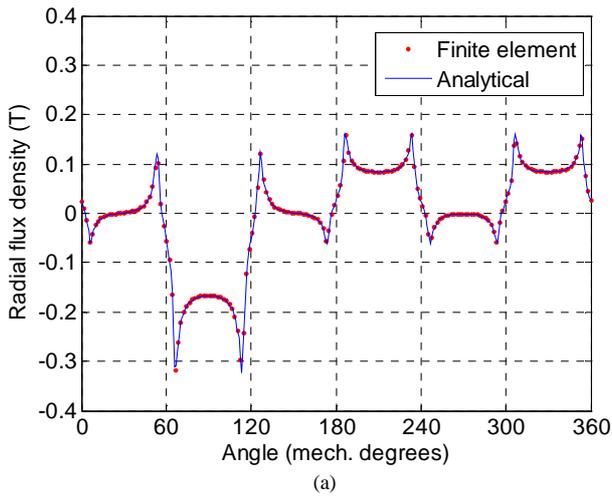
Fig. 14. Flux density distribution for radial (a) and tangential (b) component of armature reaction field in the middle of the airgap domain: J_{rms}=4.6*A/mm²*, I_a= *I* and I_b = I_c =-*I/2*, and β/δ = 0.4.
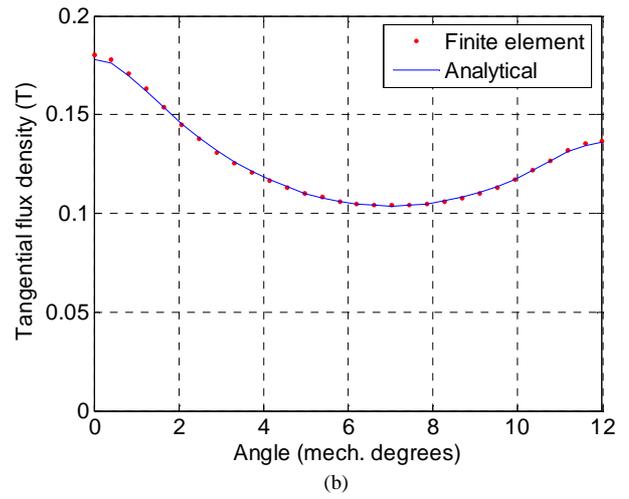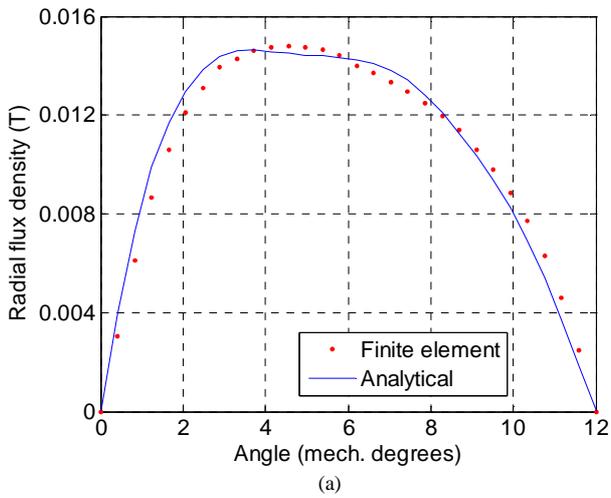

Fig. 15. Flux density distribution for radial (a) and tangential (b) component of armature reaction in the middle of the slot-opening domain for β/δ = 0.4.
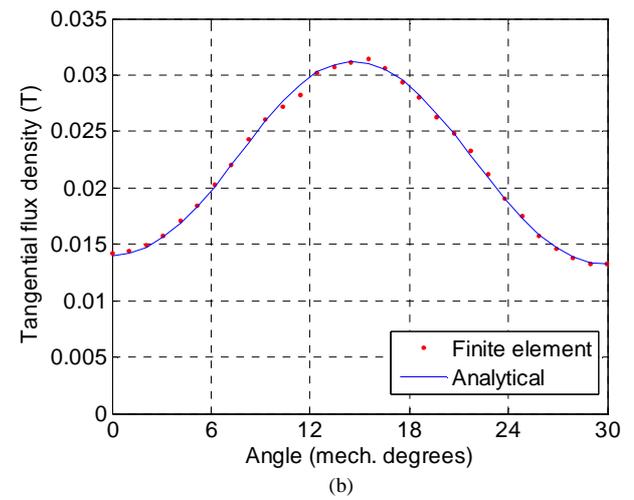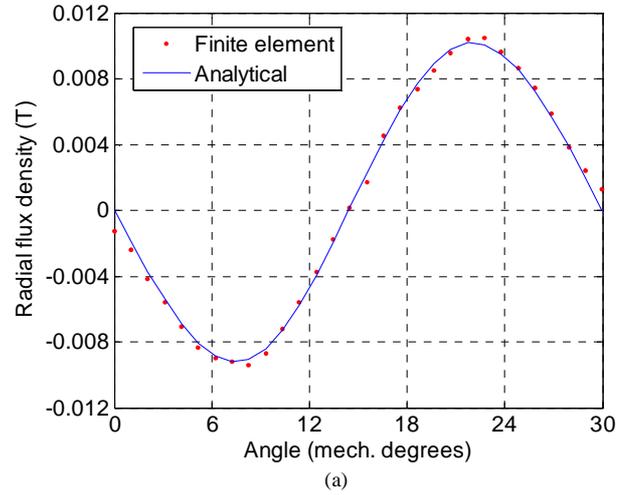

Fig. 16. Flux density distribution for radial (a) and tangential (b) component of armature reaction in the middle of the slot domain for β/δ = 0.4.

3) Results for Load Condition ($B_r = 1.2T, J_{rms} = 4.6A/mm^2$)

Figure 17 shows the flux distribution in the machine under load condition. The radial and tangential flux density distribution along a circle in the middle of the airgap under load condition ($I_a=I$ and $I_b=I_c=-I/2$) is shown in Fig. 18. The influence of the armature reaction on both the radial and the tangential flux densities is noticeable in comparison with the no-load results of Fig. 8.

The static torque versus mechanical rotor position is presented in Fig. 19 for β/δ=0.4. Compared to the FE simulations, one can see that the analytical calculation well tracks the electromagnetic torque.

Figure 20 shows the electromagnetic torque waveforms versus rotor position for different values of the slot-opening. At each rotor position, the current values in the different slots are updated to have a sinusoidal current waveform. It can be seen that the studied machine produce an average torque of about 9 Nm. The average torque decreases slightly with the slot-opening. We can also observe the effect of the slot-opening on the torque ripple. If we compare Fig. 12 and Fig. 20, it is evident that the torque ripples are mainly due to the cogging torque. Once again, it can be seen that the analytical results closely agree with the FEM results. It is worth noting that the proposed analytical model is able to predict the electromagnetic torque whatever the value of the slot-opening. This result was not possible with the previous analytical models proposed in the literature.
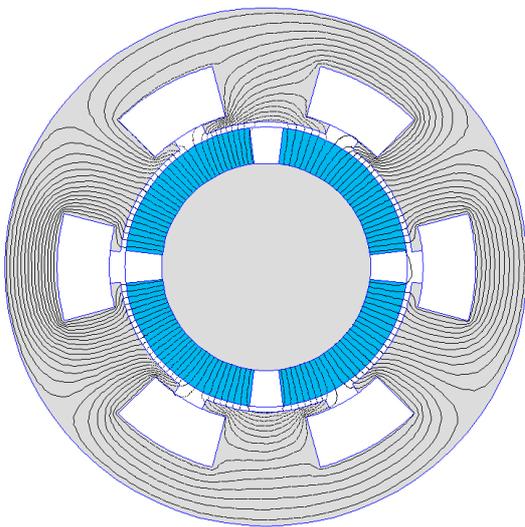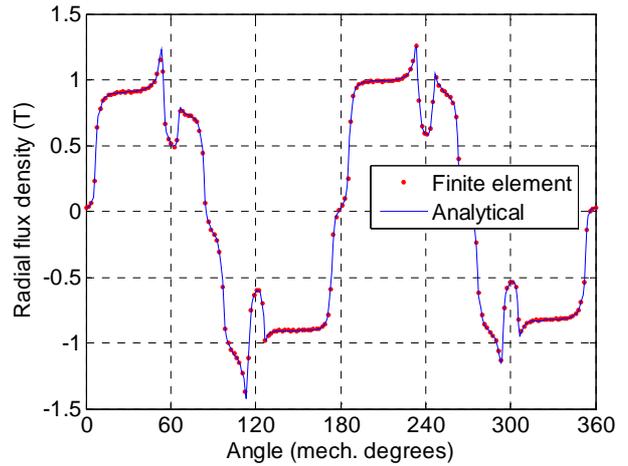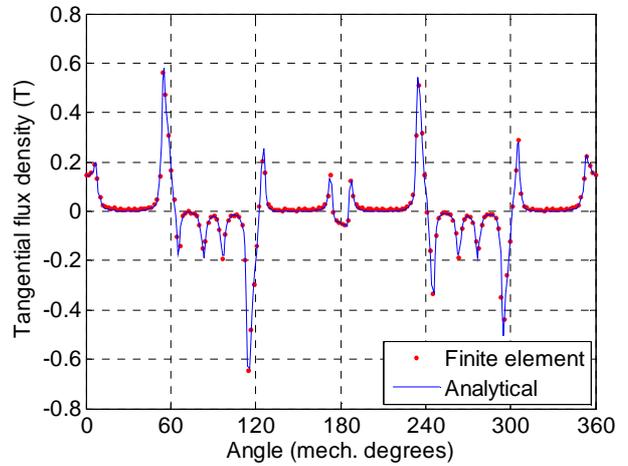

Fig. 17. Magnetic flux distribution for load condition (β/δ = 0.4).

(a)

(b)

Fig. 18. Radial (a) and tangential (b) flux density distribution in the middle of the airgap under load conditions ($\beta/\delta=0.4$)
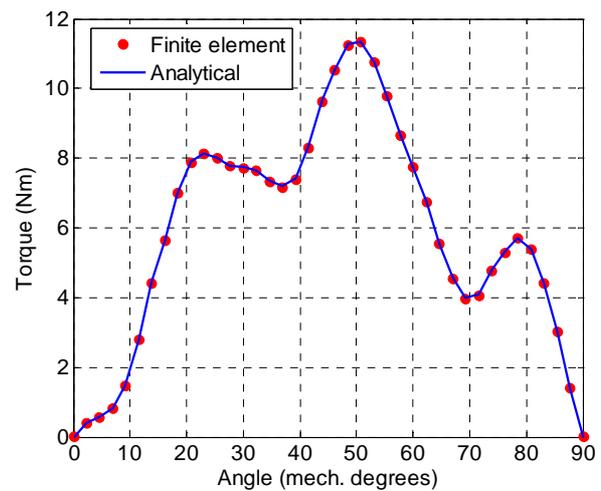

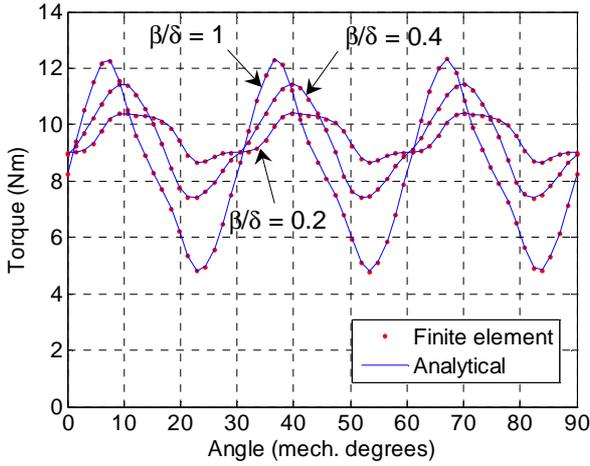Fig. 19. Static torque versus rotor position for β/δ=0.4 and J_{rms}=4.6*A/mm²*.

Fig. 20. Electromagnetic torque versus rotor position for different values of β/δ (J_{rms}=4.6A/mm²)

B. Example 2: Integer slot/pole machine (q= 2)

Another example is considered in this section for an integer slot/pole machine. This machine presents 2-pole/12-slot corresponding to a number of slot per pole and per phase equal to $q = 2$ with a single-layer winding. Notice that for this machine with $p=1$, the particular solution in the PMs region uses line 2 in (35).

The connecting matrix in this case is

$$[C] = \begin{bmatrix} 1 & 1 & 0 & 0 & 0 & 0 & -1 & -1 & 0 & 0 & 0 & 0 \\ 0 & 0 & 0 & 0 & 1 & 1 & 0 & 0 & 0 & 0 & -1 & -1 \\ 0 & 0 & -1 & -1 & 0 & 0 & 0 & 0 & 1 & 1 & 0 & 0 \end{bmatrix}$$
(47)

The geometrical parameters of the motor are given in Table II.

TABLE II
PARAMETERS OF THE INTEGER SLOT/POLE MACHINE

Symbol	Quantity	value
R_1	Inner radius of the rotor yoke	10 cm
R_2	Radius of the PMs rotor surface	11.2 cm
R_3	Stator bore radius	11.6 cm
R_4	Outer radius of the slot-opening	12 cm
R_5	Outer radius of the slot	14.5 cm
L	Axial length	40 cm
δ	Slot pitch angle	12°
β	Slot-opening angle	*variable*
α	PMs pole-arc to pole-pitch ratio	0.9
B_r	Remanence of the permanent magnets	1.2 T
p	Pole-pairs number	1
Q	Number of stator slots	12
J_{rms}	RMS current density	4.6 A/mm²

1) Results for no-load condition

Figure 21 shows the magnetic flux distribution in the machine under no-load condition. The slot-opening to slot pitch ratio is fixed to $\beta/\delta=0.6$ ($\delta = 12°$ and $\beta = 7.2°$).

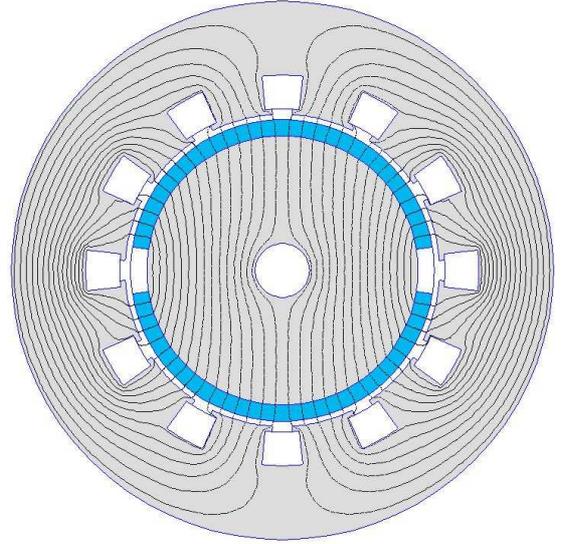Fig. 21. Magnetic flux distribution for no-load condition ($\beta/\delta = 0.6$).
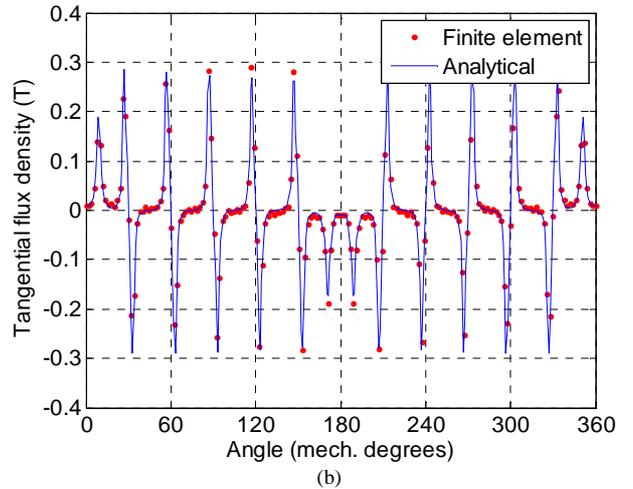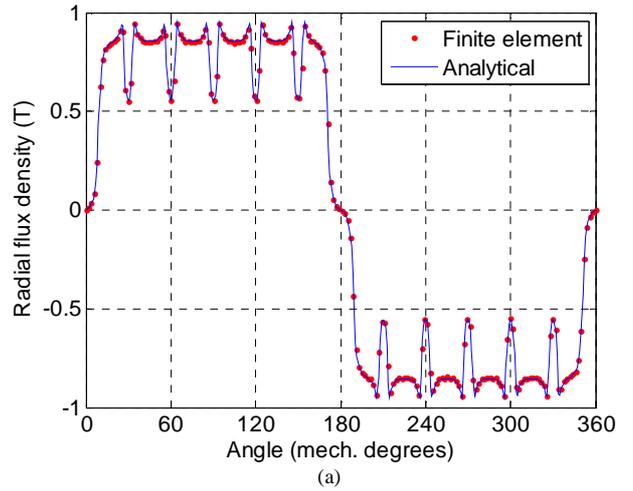

(a)

(b)

Fig. 22. Radial (a) and tangential (b) components of the flux density at no load in the middle of the airgap for $\beta/\delta = 0.6$

Figure 22 shows the flux density distribution in the middle of the airgap. Clearly, the presence of the 12 slots results in a distortion of the flux densities at the vicinity of the slot opening.

The cogging torque waveforms for several values of the slot opening *β* are given in Fig. 23. The cogging torque decreases with the slot opening. Once again, the analytical and the FE results are in good accordance.

2) Results for load condition

Figure 24 shows the flux lines in the machine under load conditions. The radial and tangential components of the airgap flux density with $I_a=I$ and $I_b=I_c=-I/2$ are shown in Fig. 25. Compared to Fig. 22, one can observe that the armature reaction have a great influence on the airgap flux density distribution.

Figure 26 shows the electromagnetic torque waveforms versus rotor position for *β/δ* = 0.6. The machine is supplied with a 3-phase sinusoidal current. It can be seen that the studied machine produces an average torque of 865 Nm. The torque ripples are due to the cogging torque but also to the space harmonics created by the stator winding distribution as well as the magnetization of the PMs. These ripples represent almost 30% of the average torque.

In order to have a good precision in the analytical torque evaluation, the number of harmonic terms used in the computations is equal to *N*=25 (airgap and PM subdomains) and *M*=*K*=15 (slots and slot-opening subdomains). For a given rotor position, the computation time is about 40 ms with the analytical model whereas the linear FEM takes about 2 s for a mesh of 23500 elements. The analytical computations being much faster, the presented model can advantageously be used in a preliminary design of PMs motors.
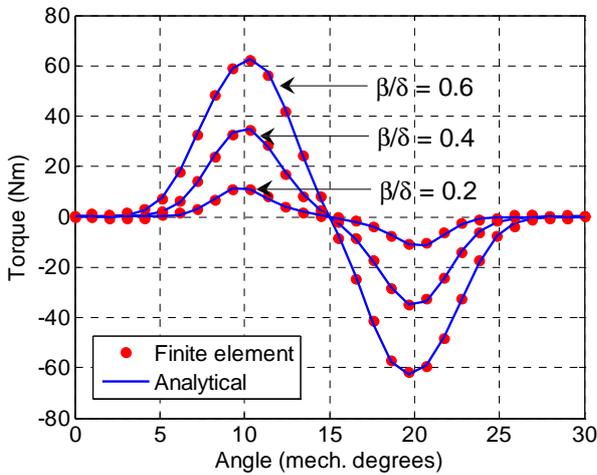

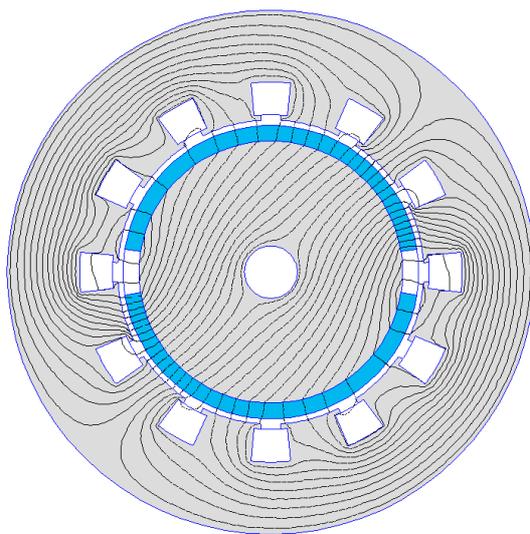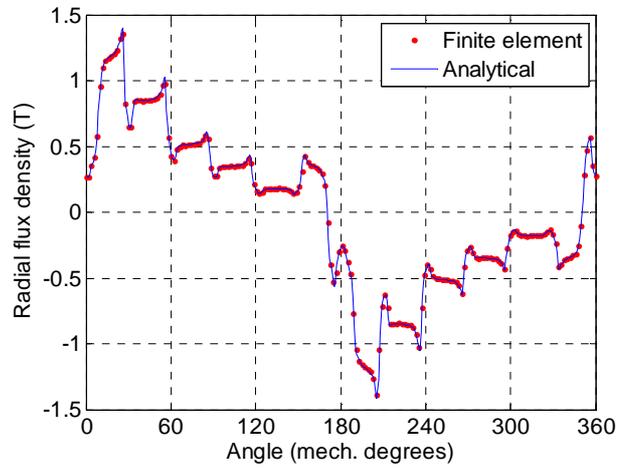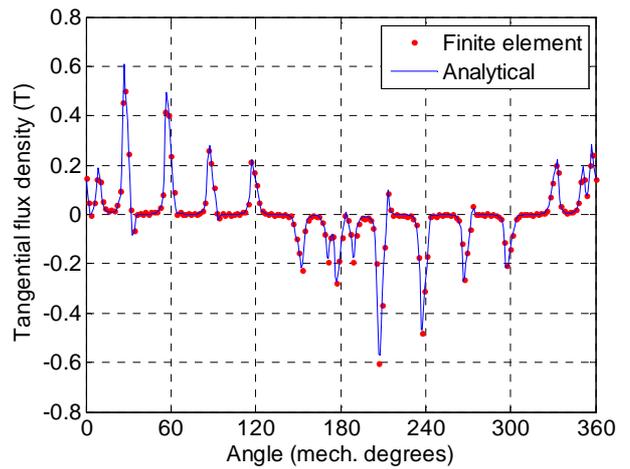Fig. 23. Cogging torque waveforms for several values of *β/δ*.

(a)

(b)

Fig. 25. Radial (a) and tangential (b) components of the airgap flux density under load conditions (*β/δ* = 0.6)

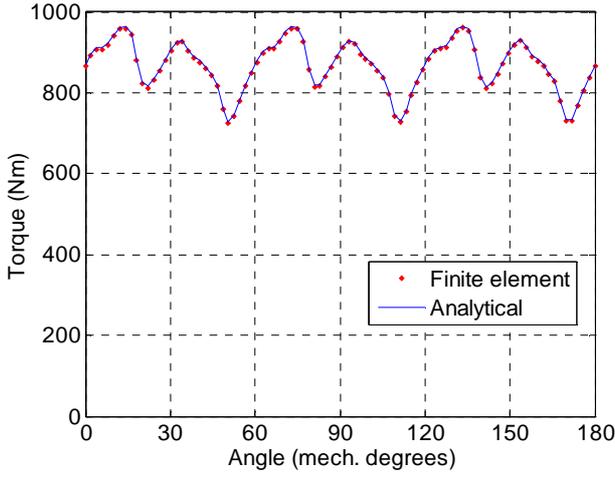Fig. 24. Magnetic flux lines under load condition (*β/δ* = 0.6)

Fig.26. Electromagnetic torque versus rotor position for β/δ=0.6 (J_{rms}=4.6A/mm²)

VI. CONCLUSION

In this paper, an exact analytical method for computing the airgap field distribution in PM motors with semi-closed slots has been presented. The Laplace's and Poisson's equations in polar coordinates have been solved by the technique of separation of variables in the different subdomains. The proposed model is sufficiently general to be used for any pole and slot combinations including fractional slot winding machines. The analytical model accounts for armature reaction field and mutual influence between slots. Flux density distribution, back-EMF and electromagnetic torque computations for no-load and load conditions are in close agreement with those issued from finite element predictions.

The analytical model developed in this paper can be used to investigate the influence of the design parameters such as slot dimensions, magnet dimensions, slot and pole number combinations or winding topologies for the calculation of PM machines performances. It presents a new tool for design and optimization of surface-mounted PM motors.

APPENDIX

For the determination of the integration coefficients, we have to calculate integrals of the form

$$f(k,n,i) = \int_{\theta_i}^{\theta_i+\beta} \cos(n\theta)\cdot\cos\left(\frac{k\pi}{\beta}(\theta-\theta_i)\right)\cdot d\theta \qquad (A.1)$$

$$g(k,n,i) = \int_{\theta_i}^{\theta_i+\beta} \sin(n\theta)\cdot\cos\left(\frac{k\pi}{\beta}(\theta-\theta_i)\right)\cdot d\theta \qquad (A.2)$$

$$r(n,i) = \int_{\theta_i}^{\theta_i+\beta} \cos(n\theta)\cdot d\theta \qquad (A.3)$$

$$s(n,i) = \int_{\theta_i}^{\theta_i+\beta} \sin(n\theta)\cdot d\theta \qquad (A.4)$$

$$F(m,k) = \int_{\theta_i}^{\theta_i+\beta} \cos\left(\frac{m\pi}{\delta}(\theta-\theta_i-\frac{1}{2}(\beta-\delta))\right)\cos\left(\frac{k\pi}{\beta}(\theta-\theta_i)\right)d\theta$$
$$(A.5)$$

The development of (A.1) and (A.2) gives the following functions that will be used in the expressions of the Fourier coefficients

- for $k\pi \neq n\beta$

$$f(k,n,i) = \frac{-n\beta^2\left((-1)^k\sin n(\beta+\theta_i)-\sin(n\theta_i)\right)}{k^2\pi^2-n^2\beta^2} \qquad (A.6)$$

$$g(k,n,i) = \frac{n\beta^2\left((-1)^k\cos n(\beta+\theta_i)-\cos(n\theta_i)\right)}{k^2\pi^2-n^2\beta^2} \qquad (A.7)$$

- for $k\pi = n\beta$

$$f(k,n,i) = \frac{\beta}{2}\left(\cos(n\theta_i)+\frac{1}{2k\pi}\left(\sin n(\theta_i+2\beta)-\sin(n\theta_i)\right)\right)$$
$$(A.8)$$

$$g(k,n,i) = \frac{\beta}{2}\left(\sin(n\theta_i)-\frac{1}{2k\pi}\left(\cos n(\theta_i+2\beta)-\cos(n\theta_i)\right)\right)$$
$$(A.9)$$

The development of (A.3) and (A.4) gives the following functions

$$r(n,i) = \frac{1}{n}\left(\sin(n\theta_i+n\beta)-\sin(n\theta_i)\right) \qquad (A.10)$$

$$s(n,i) = \frac{1}{n}\left(-\cos(n\theta_i+n\beta)+\cos(n\theta_i)\right) \qquad (A.11)$$

The development of (A.5) gives the following functions

- for $\dfrac{m\pi}{\delta} \neq \dfrac{k\pi}{\beta}$

$$F(m,k) = \frac{\frac{m\pi}{\delta}}{\left(\frac{m\pi}{\delta}\right)^2-\left(\frac{k\pi}{\beta}\right)^2}\times$$
$$\left\{(-1)^k\sin\left(\frac{m\pi}{2\delta}(\beta+\delta)\right)+\sin\left(\frac{m\pi}{2\delta}(\beta-\delta)\right)\right\}$$
$$(A.12)$$

- for $\dfrac{m\pi}{\delta} = \dfrac{k\pi}{\beta}$

$$F(m,k) = \frac{\beta}{2}\cos\left(\frac{k\pi}{2\beta}(\beta-\delta)\right) \qquad (A.13)$$

• Expressions of the coefficients A_n^{II}, B_n^{II}, C_n^{II} and D_n^{II} for the airgap subdomain

The development of (25) and (27) gives

$$A_n^{II} = A_n^I \frac{n}{R_2} \frac{E_n(R_2, R_1)}{P_n(R_2, R_1)} + X_n'(R_2)\cos(n\Delta) \tag{A.14}$$

$$C_n^{II} = C_n^I \frac{n}{R_2} \frac{E_n(R_2, R_1)}{P_n(R_2, R_1)} + X_n'(R_2)\sin(n\Delta) \tag{A.15}$$

where Δ is the PM rotor position and $X_n'(R_2) = \left.\dfrac{dX_n(r)}{dr}\right|_{r=R_2}$

$X_n(r)$ is given by (34).

The coefficient B_n^{II} and C_n^{II} defined in (26) and (28) can be written as

$$B_n^{II} = \frac{2}{2\pi} \sum_{i=1}^{Q} \int_{\theta_i}^{\theta_i+\beta} \left.\frac{\partial A_i}{\partial r}\right|_{r=R_3} \cdot \cos(n\theta) \cdot d\theta \tag{A.16}$$

$$D_n^{II} = \frac{2}{2\pi} \sum_{i=1}^{Q} \int_{\theta_i}^{\theta_i+\beta} \left.\frac{\partial A_i}{\partial r}\right|_{r=R_3} \cdot \sin(n\theta) \cdot d\theta \tag{A.17}$$

where Q is the number of stator slots. The development of (A.16) and (A.17) gives

$$B_n^{II} = \sum_{i=1}^{Q} \frac{B_0^i}{\pi R_3} \cdot r(n,i)$$
$$+ \sum_{i=1}^{Q} \sum_{k=1}^{\infty} A_k^i \frac{k}{\beta R_3} \frac{P_{k\pi/\beta}(R_3, R_4)}{E_{k\pi/\beta}(R_3, R_4)} \cdot f(k,n,i) \tag{A.18}$$
$$- \sum_{i=1}^{Q} \sum_{k=1}^{\infty} B_k^i \frac{k}{\beta R_3} \frac{2}{E_{k\pi/\beta}(R_3, R_4)} \cdot f(k,n,i)$$

$$D_n^{II} = \sum_{i=1}^{Q} \frac{B_0^i}{\pi R_3} \cdot s(n,i)$$
$$+ \sum_{i=1}^{Q} \sum_{k=1}^{\infty} A_k^i \frac{k}{\beta R_3} \frac{P_{k\pi/\beta}(R_3, R_4)}{E_{k\pi/\beta}(R_3, R_4)} \cdot g(k,n,i) \tag{A.19}$$
$$- \sum_{i=1}^{Q} \sum_{k=1}^{\infty} B_k^i \frac{k}{\beta R_3} \frac{2}{E_{k\pi/\beta}(R_3, R_4)} \cdot g(k,n,i)$$

It is worth noting that the mutual interaction between slots is related by the sum operation on Q in (A.18) and (A.19).

• Expressions of the coefficients A_n^I and C_n^I, for the PMs subdomain (36) and (37)

$$A_n^I = A_n^{II} \frac{R_2}{n} \frac{P_n(R_2, R_3)}{E_n(R_2, R_3)} + B_n^{II} \frac{R_3}{n} \frac{2}{E_n(R_3, R_2)} \tag{A.20}$$

$$C_n^I = C_n^{II} \frac{R_2}{n} \frac{P_n(R_2, R_3)}{E_n(R_2, R_3)} + D_n^{II} \frac{R_3}{n} \frac{2}{E_n(R_3, R_2)} \tag{A.21}$$

• Expression of the coefficients A_0^i, B_0^i, A_k^i and B_k^i for the *i*th slot-opening subdomain

The treatment of (11) and (12) yields to the following linear relations

$$A_k^i = \sum_{n=1}^{\infty} (A_n^{II} \frac{2R_2}{n\beta} \frac{2}{E_n(R_2, R_3)} + B_n^{II} \frac{2R_3}{n\beta} \frac{P_n(R_3, R_2)}{E_n(R_3, R_2)}) \cdot f(k,n,i)$$
$$+ \sum_{n=1}^{\infty} (C_n^{II} \frac{2R_2}{n\beta} \frac{2}{E_n(R_2, R_3)} + D_n^{II} \frac{2R_3}{n\beta} \frac{P_n(R_3, R_2)}{E_n(R_3, R_2)}) \cdot g(k,n,i) \tag{A.22}$$

$$B_k^i = \sum_{m=1}^{\infty} (A_m^j \frac{2\delta R_4}{m\pi\beta} \frac{P_{m\pi/\beta}(R_4, R_5)}{E_{m\pi/\beta}(R_4, R_5)} \cdot F(m,k) \tag{A.23}$$

The treatment of (9) and (10) yields to the following linear relations

$$A_0^i + B_0^i \ln R_3 = \sum_{n=1}^{\infty} (A_n^{II} \frac{R_2}{n\beta} \frac{2}{E_n(R_2, R_3)} + B_n^{II} \frac{R_3}{n\beta} \frac{P_n(R_3, R_2)}{E_n(R_3, R_2)}) \cdot r(n,i)$$
$$+ \sum_{n=1}^{\infty} (C_n^{II} \frac{R_2}{n\beta} \frac{2}{E_n(R_2, R_3)} + D_n^{II} \frac{R_3}{n\beta} \frac{P_n(R_3, R_2)}{E_n(R_3, R_2)}) \cdot s(n,i) \tag{A.24}$$

$$A_0^i + B_0^i \ln R_4 = A_0^j + \frac{1}{2}\mu_0 J_j \left(R_5^2 \ln R_4 - \frac{R_4^2}{2}\right) +$$
$$\sum_{m=1}^{\infty} A_m^j \frac{2R_4}{\beta} \left(\frac{\delta}{m\pi}\right)^2 \frac{P_{m\pi/\beta}(R_4, R_5)}{E_{m\pi/\beta}(R_4, R_5)} \sin\left(\frac{m\pi\beta}{2\delta}\right)\cos\left(\frac{m\pi}{2}\right) \tag{A.25}$$

• Expression of the coefficient A_m^j for the *j*th slot subdomain (18)

$$A_m^j = B_0^i \cdot \frac{4}{m\pi R_4} \sin\left(\frac{m\pi\beta}{2\delta}\right)\cos\left(\frac{m\pi}{2}\right) +$$
$$+ \sum_{k=1}^{\infty} \left(A_k^i \frac{2}{E_{k\pi/\beta}(R_3, R_4)} - B_k^i \frac{P_{k\pi/\beta}(R_4, R_3)}{E_{k\pi/\beta}(R_3, R_4)}\right) \cdot \frac{2k\pi}{\delta\beta R_4} \cdot F(m,k) \tag{A.26}$$

We have to solve a system of linear equations with the same number of unknowns. By rewriting the above equations in matrix and vectors format, a numerical solution can be found by using mathematical software (Matlab).

REFERENCES

[1] Z. J. liu, and J. T. Li, "Analytical solution of air-gap field in permanent magnet motors taking into account the effect of pole transition over slots," *IEEE Trans. Magn.,* vol. 43, no. 10, pp. 3872-3882, Oct. 2007.

[2] F. Dubas, and C. Espanet "Analytical solution of the magnetic field in permanent-magnet motors taking into account slotting effect: no-load vector potential and flux density calculation," *IEEE Trans. Magn.,* vol. 45, no. 5, pp. 2097-21092, May 2009.

[3] Z. Q. Zhu, L. J. Wu, and Z.P. Xia, "An accurate subdomain model for magnetic field computation in slotted surface-mounted permanent magnet machines," *IEEE Trans. Magn.,* vol. 46, no. 4, pp. 1100-1115, Apr. 2010.

[4] F. M. Sargos and A. Rezzoug, "Analytical calculation of airgap magnetic field produced by inset permanent magnet rotor machine," *J. Physics III* (in French), vol. 1, pp 103-110, 1990.

[5] Z. Q. Zhu and D. Howe, "Instantaneous magnetic-field distribution in brushless permanent-magnet dc motor, part III: Effect of slotting," *IEEE Trans. Magn.,* vol. 29, no. 1, pp. 143-151, Jan. 1993.

[6] D. Zarko, D. Ban, and T. A. Lipo, "Analytical calculation of magnetic field distribution in the slotted air gap of a surface permanent-magnet motor using complex relative air-gap permeance," *IEEE Trans. Magn.,* vol. 42, no. 7, pp. 1828-1837, Jul. 2006.

[7] M. Markovic, M. Jufer, and Y. Perriard, "Reducing the cogging torque in brushless dc motors by using conformal mappings," *IEEE Trans. Magn.,* vol. 40, no. 2, pp. 451-455, Mar. 2004.

[8] K. Boughrara, D. Zarko, R. Ibtiouen, O. Touhami, and A. Rezzoug, "Magnetic field analysis of inset and surface-mounted permanent-magnet synchronous motor using Schwarz-Christoffel transformation," *IEEE Trans. Magn.,* vol. 45, no. 8, pp. 3166-3168, Aug. 2009.

[9] Q. Gu and H. Gao, "Effect of slotting in PM electrical machines," *Elect. Mach. Power Syst.,* vol. 10, pp. 273-284, 1985.

[10] N. Boules, "Prediction of no-load flux density distribution in permanent magnet machines," *IEEE Trans. Ind. Appl.,* vol. IA-21, no. 3, pp. 633-643, Jul./Aug. 1985.

[11] B. Ackermann and R. Sottek, "Analytical modeling of the cogging torque in permanent magnet motors," *Elect. Eng.,* vol. 78, no. 2, pp. 117-125, Mar. 1994.

[12] Z. Q. Zhu, and D. Howe, "Analytical prediction of the cogging torque in radial-field permanent magnet brushless motors," *IEEE Trans. Magn.,* vol. 28, no. 2, pp. 1371-1374, Mar. 1992.

[13] K. F. Rasmussen, H. D. John, T. J. E. Miller, M. I. McGilp, and O. Mircea, "Analytical and numerical computation of air-gap magnetic field in brushless motors with surface permanent magnet," *IEEE Trans. Magn.,* vol. 36, no. 6, pp. 1547-1554, Nov./ Dec. 2000.

[14] X. Wang, Q. Li, S. Wang, and Q. Li, "Analytical calculation of air-gap magnetic field distribution and instantaneous characteristics of brushless dc motors," *IEEE Trans. Energy. Convers.,* vol. 18, no. 3, pp. 424432, Sep. 2003.

[15] P. Kumar, and P. Bauer, "Improved analytical model of a permanent-magnet brushless DC motor," *IEEE Trans. Magn.,* vol. 44, no. 10, pp. 2299-2309, Oct. 2008.

[16] Z. J. liu, and J. T. Li, "Accurate prediction of magnetic field and magnetic forces in permanent magnet motor using an analytical solution," *IEEE Trans. Energy. Convers.,* vol. 23, no. 3, pp. 717-726, Sept. 2008.

[17] B. N. Cassimere, S. D. Sudhoff, and D. H. Sudhoff "Analytical design model for surface mounted permanent-magnet synchronous machines," *IEEE Trans. Energy Convers.*, vol. 24, no. 2, pp. 347–357, June 2009

[18] A. Bellara, Y. Amara, G. Barakat, and B. Dakyo, "Two-dimensional exact analytical solution of armature reaction field in slotted surface mounted PM radial flux synchronous machines," *IEEE Trans. Magn.,* vol. 45, no. 10, pp. 4534-4538, Oct. 2009.

[19] B. L. J. Gysen, K. J. Meessen, J. J. H. Paulides, and E. A. Lomonova, "General formulation of the electromagnetic field distribution in machines and devices using Fourier analysis," *IEEE Trans. Magn.,* vol. 46, no. 1, pp. 39-52, Jan. 2010.

[20] T. Lubin, S. Mezani, and A. Rezzoug, "Exact analytical method for magnetic field computation in the air-gap of cylindrical electrical machines considering slotting effects," *IEEE Trans. Magn.,* vol. 46, no. 4, pp. 1092-1099, Apr. 2010.

[21] A. M. El-Refaie, "Fractional-slot concentrated-windings synchronous permanent magnet machines: opportunities and challenges," *IEEE Trans. Ind. Electron,* vol. 57, no. 1, pp. 107-121, Jan. 2010.

[22] D. Ishak, Z. Q. Zhu, and D. Howe, "Eddy-current loss in the rotor magnets of permanent-magnet brushless machines having a fractional number of slots per pole," *IEEE Trans. Magn.,* vol. 41, no. 9, pp. 2462-2469, Sep. 2005.

[23] N. Bianchi, and E. Fornasiero "Impact of MMF space harmonic on rotor losses in fractional-slot permanent-magnet machines," *IEEE Trans. Energy Convers.*, vol. 24, no. 2, pp. 323–328, June 2009

[24] S. J. Farlow, *Partial Differential Equations for Scientists and Engineers.* Dover publications, New York, 414 pp, 1993.

[25] D. C. Meeker, "Finite Element Method Magnetics", *Version 4.2 (1 April 2009 Build)*, http://www.femm.info

Thierry Lubin was born in Sedan, France, in 1970. He received the M.S. degree from the University of Paris 6, France in 1994 and the Ph.D. degree from the University Henri Poincaré, Nancy, France, in 2003.

He is currently a lecturer of Electrical Engineering at the University of Nancy at the Groupe de Recherche en Electrotechnique et Electronique de Nancy. His interests include modeling and control of electrical machines and applied superconductivity in electrical devices.

Smail Mezani was born in Algiers, Algeria, in 1974. He received the engineer diploma and the magister degree from the University of Sciences and Technology Houari Boumediene, Algiers, Algeria in 1996 and 1999 respectively. He obtained the Ph.D. degree from the Institut National Polytechnique de Lorraine, France, in 2004.

He is currently a lecturer at the University Henri Poincaré of Nancy, France, at the Groupe de Recherche en Electrotechnique et Electronique de Nancy where his research interests include the applications of superconductors in electromechanical devices.

Abderrezak Rezzoug received the electrical engineer degree from ENSEM INPL, Nancy, France in 1972, and the Dr. Ing. diploma and the Ph.D. degree from INPL, in 1979 and 1987 respectively.

After working at the INPL as an assistant Professor until 1991, he is currently a Professor of Electrical Engineering at the University Henri Poincaré, Nancy, France. As a member of the Groupe de Recherche en Electrotechnique et Electronique de Nancy, his main subjects of research concern superconducting applications to electrical devices, and the control and diagnosis of electrical machines.